Ceramics International 49 (2023) 15091–15100

Contents lists available at ScienceDirect

Ceramics International

journal homepage: www.elsevier.com/locate/ceramint

Enhanced tribological behavior of VAlN hard ceramic coating with intermittent amorphous carbon layer

Yupeng Zhang [a,b], Zhenyu Wang [a,b], Peng Guo [a,b], Aiying Wang [a,b], Peiling Ke [a,b,*]

[a] Key Laboratory of Marine Materials and Related Technologies, Zhejiang Key Laboratory of Marine Materials and Protective Technologies, Ningbo Institute of Materials Technology and Engineering, Chinese Academy of Sciences, Ningbo, 315201, China
[b] Center of Materials Science and Optoelectronics Engineering, University of Chinese Academy of Sciences, Beijing, 100049, China

ARTICLE INFO

Handling Editor: Dr P. Vincenzini

Keywords:
VAlN hard coating
a-C film
Friction coefficient
Lubricating phase
Transfer film

ABSTRACT

Long-term lubricate coatings over a wide temperature range are prerequisite and still facing open challenge for aero-engines and sliding components in harsh conditions. In this work, DC magnetron sputtered VAlN hard ceramic coating was modified by the subsequently post-annealing treatment with graphite powder, where the intermittent amorphous carbon (a-C) top-layer was achieved under temperature of 800 °C and high vacuum. The tribological behavior of modified VAlN coatings was investigated and the results showed that displayed the high hardness of 34.4 GPa and the excellent self-adaptive lubrication from room temperature to 600 °C. Especially, due to the benefits of lamellar sliding interface between a-C top-layer and the a-C transfer film (30 nm–68 nm), the modified coating behaved the lowest friction coefficient of 0.11 at 300 °C. However, increasing the temperature to 600 °C led to the increased and stabilized friction coefficient at 0.36–0.41, which could be attributed to the formation of V_2O_5 lubricating phase. Further insight into the tribological behavior of the modified VAlN coating by a-C top-layer was discussed in terms of the microstructure evolution during friction test.

1. Introduction

The application of aerospace and mechanical devices over a wide temperature range is still facing the challenge of gradual wear-out and friction damage that can cause parts failure and serious accident [1–3]. For satisfying the specificly functional requirements in high-temperature mechanical system, the coatings such as $(Al,Cr)_2O_3$, VN, Cr_2N, MAX phase (Cr_2AlC, V_2AlN, etc.) and other oxide/nitride have been developed and prepared through magnetron sputtering, arc ion plating, thermal spraying and other technologies [4,5]. However, these coatings are prone to worn due to the tribo-chemical reaction with changes of phase and composition structure over wide temperature range (25 °C–800 °C), where the high friction coefficient (COF) and short wear-life with poor temperature adaptability are always observed [6–9]. To solve these problems, it is necessary to develop the advanced coating materials together with excellent toughness, low COF and long wear-life under conditions of wide temperature range.

The VN is carefully considered as a suitable basal component due to its self-lubricating performance, which is easily oxidized to form the V_2O_5 (Magneli phase) to reduce the COF at high temperature (450 °C–700 °C) [10,11]. However, the stability, friction and wear performance of VN are unsatisfactory, due to the high COF below 450 °C and easy consumption of V_2O_5 above 650 °C, therefore, by doping Al, C elements to design the interlayer structure and prepare composite coating to enhance its oxidation resistance, hardness and reduce its COF [12,13]. For instance, the hardness and oxidation resistance of VN coating can be greatly improved after adding Al element by direct current magnetron sputtering (DCMS), and even high dense and hardness (40 GPa) of $V_{0.48}Al_{0.52}N$ phase can be achieved [14,15]. Different content of Al element in VAlN coating may affect growth structure and form columnar, fibrous and columnar crystal structure, meanwhile, the $V_{1-x}Al_xN$ coating with excellent mechanical properties of high hardness and strong adhesion can be obtained by adjusting the Ar/N_2 flow rate and bias voltage [12,16]. It is a new method to implanted the high-density Al^+ into c-VN to form supersaturated c-VAlN with an Al content up to 84% in the cationic lattice by high-power pulsed magnetron sputtering (HiPIMS), which can improve the high temperature oxidation resistance of coating [17,18].

While, the COF of VAlN coating is very high from room temperature (RT, 25 °C) to medium temperature because lack of lubricating phase,

* Corresponding author. Key Laboratory of Marine Materials and Related Technologies, Zhejiang Key Laboratory of Marine Materials and Protective Technologies, Ningbo Institute of Materials Technology and Engineering, Chinese Academy of Sciences, Ningbo, 315201, China.
E-mail address: kepl@nimte.ac.cn (P. Ke).

https://doi.org/10.1016/j.ceramint.2023.01.092
Received 4 November 2022; Received in revised form 21 December 2022; Accepted 11 January 2023
Available online 12 January 2023

thus introducing the lubricating phase is essential for achieving the low COF. As a self-lubricating solid material, a-C film could be a suitable candidate for acquiring excellent tribological property from RT to medium temperature. For instance, The reactive molecular dynamics simulation was used to investigate the friction mechanism of a-C film, and found the key point of the obtained low COF is attributes to the passivation of a-C dangling bonds and graphitized structure [19], which is consistent with the fact that the low COF (0.16) of a-C film is obtained in the atmospheric environment, due to the free σ-bonds of surface carbon atoms are passivated or terminated by oxygen [20]. By adjusting the duct bias voltage to control the defects of a-C film can reduce the COF to 0.13 at RT, meanwhile, the current-carrying COF of a-C film is decreased from 0.2 to 0.03 with the current increase due to the transfer film of graphene nanosheets during the sliding process [21,22]. An onion like structure of the a-C embedded with Mo and W carbides nano-crystallites show a low COF (0.15–0.25) owing to the formation of stability tribo-layer at RT [23]. Therefore, the advantage of a-C film may be more exerted after assembling it on the VAlN hard coating surface to acquire excellent tribological property over wide temperature range. In the current research, the introduction of C by magnetron sputtering will form the carbide phase within the coatings, which cannot fully play the lubricating advantage. Moreover, the thermal stability of a-C film itself prepared by magnetron sputtering is insufficient and even the formed carbide phase normally has high COF at high temperature (>400 °C), and the oxidized carbide phase will damage the high temperature performance of coating [24]. So far, it is still a difficulty and challenge to prepare wide-temperature range coatings with a-C film onto the surface, and then realize comprehensive excellent performance such as high hardness, good toughness, low COF and high wear resistance [25]. Besides, limited progress has been made on the tribological performance of VAlN over wide temperature range, as well as the evolution of its composition, structure and lubrication mechanism is worth to be reported and revealed.

In this article, the DCMS technology is performed to deposit the VAlN hard ceramic coating, and then the a-C top-layer with high thermal stability is grown onto the coating surface through a post-annealing treatment with graphite powder, which is conducive to form the lubricating layer in the process of low and medium temperature friction. Thus an excellent solid lubricating coating with good mechanical properties, wear resistance and low COF ranging from 25 °C to 600 °C is achieved, and its lubrication mechanism over wide temperature range is also discussed.

2. Experimental

2.1. Preparation of VAlN coating

The home-made DCMS technology was used to deposit coatings on Si wafers (p-100) and Ni-based superalloy (GH3600) substrates as shown in Fig. 1. The substrates were ultrasonically clean with acetone and anhydrous ethanol for 10 min before deposition. The equipment was heat to 400 °C to remove gas impurities and water vapor adsorbed on substrates. The Ar (20 sccm) was introduced as ion source to etch substrates for 30 min with a pulse bias of −400 V. Connect the pulse negative bias (−150 V) with substrate, turn on the Ti target baffle to deposit the transition layer (30 min) under DC power of 90 W. Subsequently, N_2 with a flow rate of 5 sccm was introduced, and the DC power (150 W) of the V/Al composite target was turned on to deposit for 180 min. By adjusting the valve to control the working pressure and VAlN coatings were named S1 (0.7 Pa), S2 (0.6 Pa), S3 (0.5 Pa) and S4 (0.4 Pa). Take out coatings after the chamber temperature drops to RT.

The post-annealing of coatings were performed in the tube furnace with graphite powder in corundum crucible as shown in Fig. 1 under the condition of 800 °C and 9×10^{-4} Pa for 1.5 h. Finally, take out the coatings after the tube furnace lowered to RT. The coating prepared for comprising in the work pressure of 0.5 Pa without annealing was named S5.

2.2. Tribological test

The high-temperature ball-on-disk tribometer (Anton paar) was used to investigate the tribological performance of coatings at 25 °C, 300 °C and 600 °C, respectively. The counterpart ball is Al_2O_3 (Φ = 6 mm), the rotation speed, load, radius and sliding distance are 20 rpm, 2 N, 5 mm and 20 m, respectively. Normalized wear rates (W_R, $mm^3N^{-1}m^{-1}$) were calculated by the following equation [26]:

$$W_R = \frac{2\pi rd\left(3d^2 + 4b^2\right)}{6bF_N L}$$

The d, b and r in the equation are the depth, width, radius of the wear track, respectively; the F_N and L are the normal load and sliding distance, respectively. The W_R of coatings obtained are average value after calculations of different positions on the wear track.

2.3. Microstructural characterization

The cross-sectional and surface morphology of coatings are observed by the field emission scanning electron microscope (SEM, Hitachi S4800). The nanoindenter (MTS NANO G200) is to detect the hardness, toughness of coatings. The X-ray diffractometer (XRD, M03XHFMXP3, Mac Science) and laser Raman spectroscopy (Renishaw, inVia-reflex, excitation wavelength is 532 nm) are to analyze the crystal plane phase structure of coatings. The depth and width of wear track were measured by a surface profilometer (Alpha-Step IQ, America) to calculate wear rate. The chemical element valences of coatings are determined by X-ray photoelectron spectroscope (XPS, PHI-5702, Al Kα X-ray source), the binding energy of the carbon contaminant (C1s = 284.8 eV) is used to calibrate as reference. Cross-sectional specimen was prepared

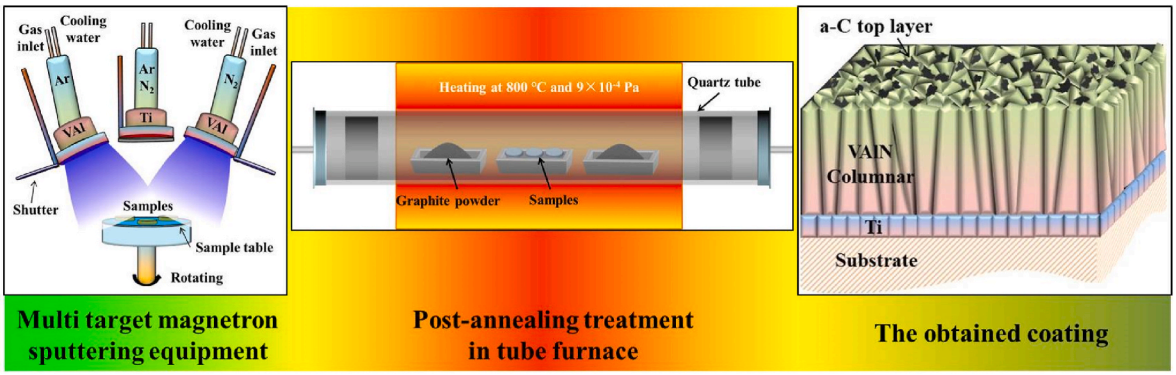

Fig. 1. The deposition and post-annealing treatment procedure of prepared coatings.

by the Focused Ion Beam (FIB, Helios-G4-CX), and the Transmission scanning electron microscope (TEM, FEI, Talos F200x) was used to characterize the microstructure of coating.

3. Results and discussion

3.1. Mechanical properties and structural of coatings

The hardness (H) and elastic modulus (E) of S1–S4 coatings were increased with the decreased working pressure as shown in Fig. 2 (a). The lowest H (20.9 GPa) and E (341 GPa) of S1 was obtained when the working pressure was 0.7 Pa. While the working pressure lowered to 0.4 Pa, the highest H (34.4 GPa) and E (472 GPa) of the S4 was reached, which may be the reduced impurity atoms and tighter bonding formed between deposited atoms at the lower working pressure. In addition, the S5 without post-annealing possess the lower H and E than S3, in which the mechanical properties of ceramics coatings may be enhanced by annealing at high temperature and vacuum. The H/E and H^3/E^2 represent fracture toughness of coatings [27,28], and the coating S3 with a working pressure of 0.5 Pa has the highest H/E and H^3/E^2 among the annealed coatings shown in Fig. 2 (b), indicating that has better mechanical properties and toughness. Thus, the following characterization will be represented by S3.

The working pressure will be a key factor effecting cross-sectional and surface morphology of coating. The thickness of the coating is about 1.43–1.47 μm. The Ti transition layer with dense structure is about 0.3 μm, which is to increase the adhesion strength between the coating and Ni-based superalloy substrate. The S1 coating shows typical columnar crystal morphology with relatively large diameter and chink in Fig. 2 (c), and the coating surface shows irregular triangular cone-shaped protrusions in Fig. 2 (d). As a contrast, the S3 coating presents the uniform, finer and denser columnar crystalline in Fig. 2 (e), and a relatively flat surface with round protrusions in Fig. 2 (f). The content of elements in the VAlN coating listed in Fig. 2 (d) and (f), in which the ratio of V/Al is close to 1 and the content of C element are different in each coatings.

3.2. The phase structure analysis of coatings

The XRD pattern shows the same diffraction peak under different working pressure in Fig. 3 (a). The diffraction peaks located at 36.1° (002), 37.9° (101) and 81.1 (202) are belong to hexagonal AlN phase (ICDD#00-025-1133). The diffraction peak at 37.9° (111) is assigned to the cubic VN phase (ICDD#04-004-5182), and the diffraction peaks located at 41.9° (111), 81.1° (221) are belong to the hexagonal V_2N (ICDD#00-032-1413). Obviously the preferred orientation of AlN (101) coincides with VN (111) results in the higher intensity at 37.9°, and the crystallinity of AlN phase is higher than VN then conducive to the enhanced hardness.

Raman spectrum of coatings is shown in Fig. 3 (b). The characteristic peaks in the region of 100–800 cm^{-1} correspond to the VAlN coating. In addition, for annealed coatings, a typical disorder (D) peak at 1345 cm^{-1} is the breathing mode derived from the sp^2 bond in the aromatic ring, and a typical graphitic (G) peak at 1606 cm^{-1} is derived from the sp^2 bond of stretching vibration in rings and chains of graphite-like phase carbon [25,29]. This suggests that during the 800 °C and high vacuum

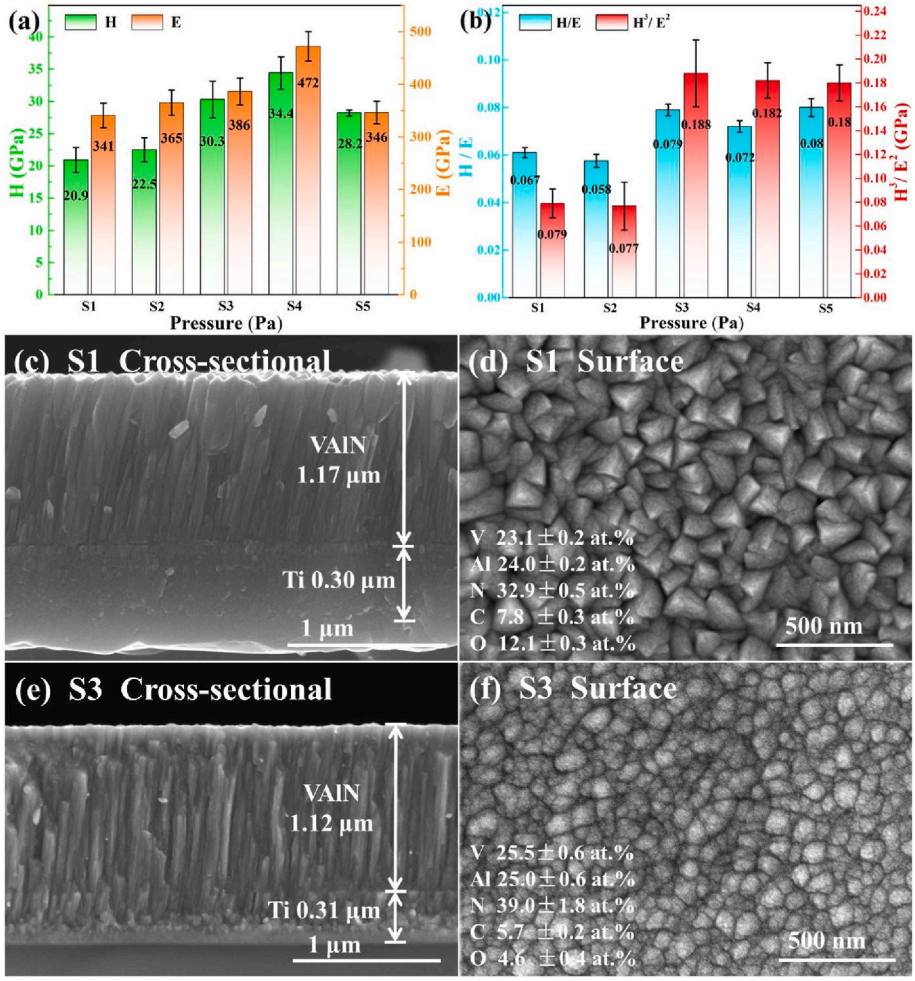

Fig. 2. Mechanical properties of coatings (a), (b); microstructural of S1 (c), (d) and S3 (e), (f).

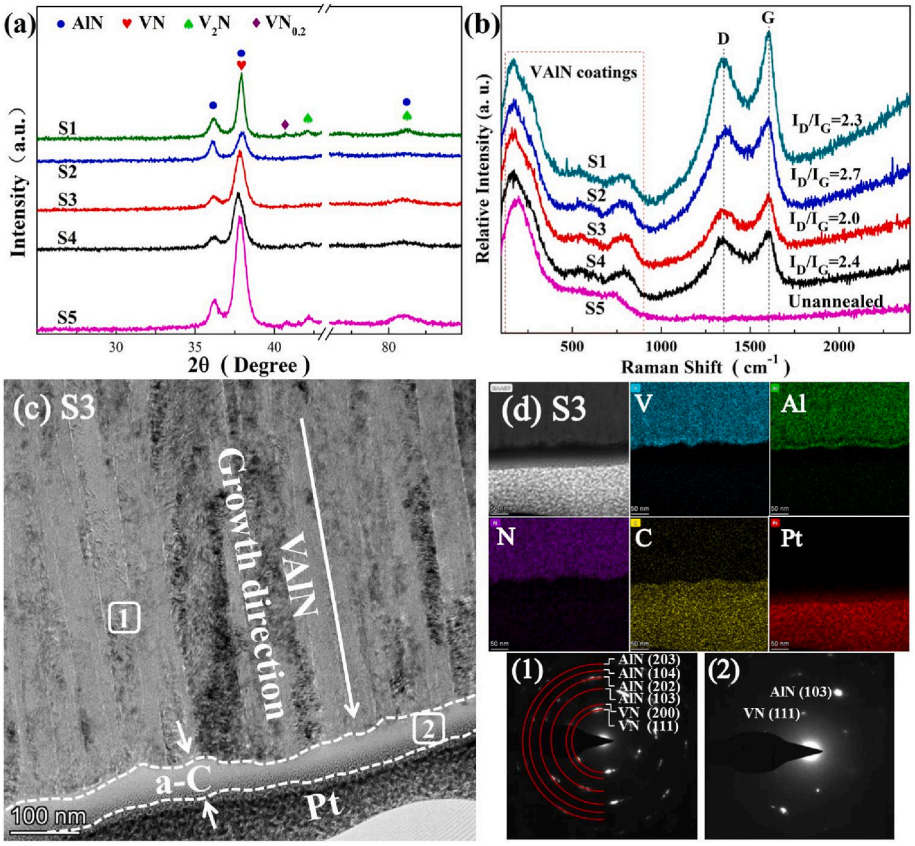

Fig. 3. The XRD (a) and Raman (b) patterns of different coatings at RT, the cross-sectional TEM (c), the mapping and SAED (d) of the coating S3.

post-annealing process, trace amount of C atoms escape from the graphite powder in gaseous to form the intermittent a-C top-layer on the VAlN coating surface. For comparison, the un-annealed coating S5 did not form characteristic peaks of a-C. The intensity ratio of D peak to G peak (I_D/I_G) is proportional to the sp^2/sp^3 content of carbon atoms, the coating is mainly composed of sp^2 bonds of the graphite-like phase when $I_D/I_G > 3.0$ in a-C film [23]. Generally, the decrease of I_D/I_G ratio means a decrease in the number or size of graphitic domains, the content of sp^3

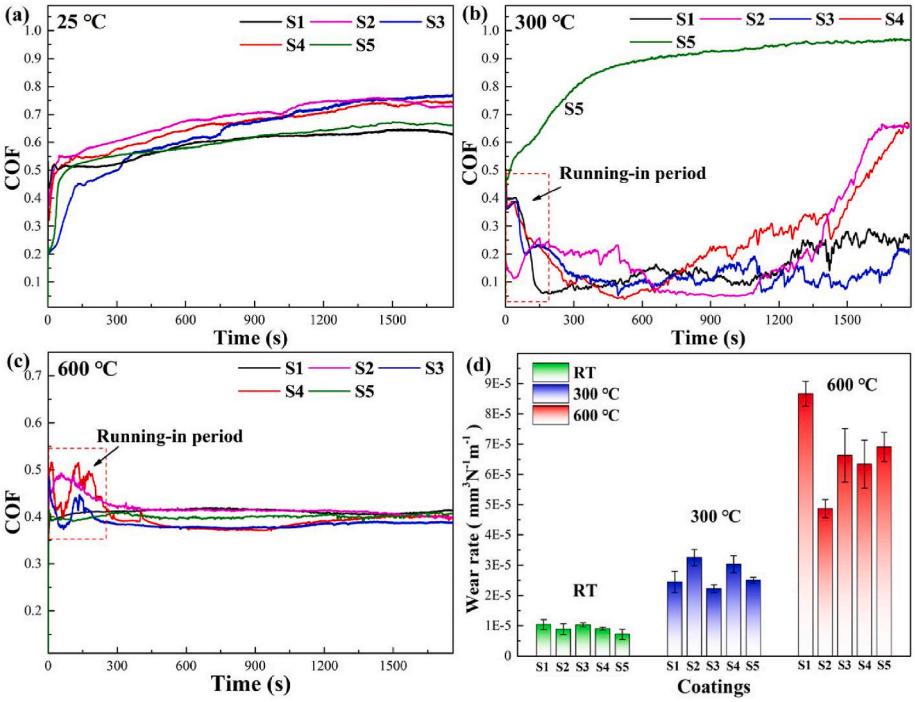

Fig. 4. The friction curves of coatings at 25 °C (a), 300 °C (b), 600 °C (c) and the wear rates (d) of coatings.

bonds will increase (sp^2 decrease), and the formation of sp^3 clusters lead to an increase of the hardness and wear resistance in a certain extent [30,31]. The $I_D/I_G < 3.0$ in four samples indicate that a certain amount of sp^3 hybrid a-C is formed in the coating. It can be seen from the above characterization that the modified VAlN coating was successfully prepared by DCMS technology and post-annealing.

The TEM was used to observe the presence of a-C top layer and microstructure of the post-annealed S3 coating. It can be seen from Fig. 3 (c) and (d) that the a-C top-layer with thickness of 40 nm–52 nm is distributed onto the VAlN coating surface. A certain amount of Pt penetrates into the loose a-C film during the FIB process. The selected area electron diffraction (SAED) marked (1) in Fig. 3 (d) shows the crystalline phase of the VAlN coating, the mainly crystalline phase are VN and AlN detected at position of box (1), and SAED marked (2) shows the amorphous phase of the a-C top-layer detected at position of box (2). This result corresponds to the results of Fig. 3 (b) sufficiently demonstrate that the a-C film is successfully formed on the coating surface.

3.3. Tribological behavior of coatings

In Fig. 4 (a), the COF range from 0.55 to 0.75 of coatings illustrate that the modified VAlN hard ceramic coatings can remarkably reduce COF at RT. Since the cone-shaped protrusions on the surface are not easily oxidized and damaged at RT, then the point contact and two hard contact interfaces during friction test result in a relatively high COF. The COF is relative high in the running-in period at 300 °C as shown in Fig. 4 (b), subsequently all friction curves show a downward trend. The S1 and S3 show the best friction behavior and the COF are stable at 0.15 and 0.11, respectively. The COF curves of S2 and S4 are gradually increasing in the end of friction process. Especially the S5 without a-C top-layer exhibited extremely high COF of about 0.93 during the friction at RT. Comparing all the friction curves at 300 °C, the COF of S4 possesses the lowest COF of 0.04 in the middle friction but S1 and S3 possess lower COF and relative stable curves during the whole friction process, which highlights the excellent lubricating behavior of a-C film. In the high temperature friction of 600 °C as shown in Fig. 4 (c), the COF is relative high and unstable on the running-in period, and after that the COF of coatings are stable between 0.36 and 0.41, thus endows the coating with self-adaptive lubricating behavior. The above COF curves show that the lubricating effect of a-C film at 300 °C is more obvious over a wide temperature range.

The corresponding W_R of coatings over a wide temperature range have been tested and compared with each other in Fig. 4 (d). The results show that the trend of W_R was rising as the temperature increasing, and the minimum W_R was obtained at RT due to the high hardness of coatings, subsequently the W_R was gradually rising with the increasing of temperature to 300 °C that can promote the formation of a-C transfer film since the wear debris agglomeration on the contact surface of counterpart ball [32]. The maximum W_R was achieved at high temperature of 600 °C due to the relatively loosen coating surface caused by the tribochemical reaction.

3.4. Phase structure and Raman analysis after friction test

The S3 coating was characterized by XRD and Raman to investigate the change of phase structure before and after friction test at RT, 300 °C and 600 °C. After friction at 300 °C, the phase structure of AlN and VN are almost unchanged in Fig. 5 (a), indicating that the VAlN underlayer is not destroyed significantly in the friction process from RT to 300 °C, which could provide support to bear the applied load and prevented the coating from peeling off and rapidly failure. With the temperature increased to 600 °C, the AlN phase at 37.9° is remain on high intensity and only few was oxidized, thus the diffraction peaks appear at 21.6°, 27.6° and 34.8° is belong to Al_2O_3 (ICDD#00-021-0010) in Fig. 5 (a), which indicated that the oxidation resistance temperature of hexagonal AlN is above 600 °C. However, VN is oxidized to a large amount of vanadium oxide, the diffraction peak of V_2O_5 lubricating phase marked as orange triangle are located at 15.3°, 20.3°, 26.1°, 31°, 32.4°, 34.3°, 36° (ICDD#00-041-1426) in Fig. 5 (a). In addition, the diffraction peaks of VO_2 was observed at 27.7°, 33.4°, 39.1°, 42.1° (ICDD#00-034-0187).

The structural change of a-C top-layer can be confirmed from the Raman pattern in Fig. 5 (b), both the content of D peak and G peak have minor changed during the friction from 25 °C to 300 °C. During the friction process at 25 °C, only trace amount of a-C film accumulated on the wear track, and the relative sliding between hard ceramics results in high COF. However, the I_D/I_G increased to 2.2 during the friction process at 300 °C caused by the increased content of D peak at 1379 cm^{-1} along with declined content of G peak at 1588 cm^{-1}, which indicate that the a-C top-layer was slightly graphitized [32,33] and accompanied with the reduced COF. For comparison, the COF of coating S5 is extremely high at 300 °C. That is factoring in absence of a-C top-layer as lubricating phase, and the VO_2 is generated on the nitride coating surface as a hard abrasive particle to cause the abrasive wear [34]. Simultaneously, the phase V_2O_5 appears at 284 cm^{-1}, 33.5 cm^{-1}, 405 cm^{-1}, 529 cm^{-1}, 709 cm^{-1}, 995 cm^{-1} after friction test at 600 °C, and the characteristic peaks at 144 cm^{-1}, 195 cm^{-1}, 482 cm^{-1} were identified the phase VO_2, while the peaks of a-C film was oxidized and disappeared [35]. This proved that the formed V_2O_5 during the friction process at 600 °C is the main lubricating phase and contributes to the low COF.

3.5. XPS analysis after friction test

Combined with XPS analysis, the valence state and bonding mode of elements in the coating can provide a deep understanding of mechanism. Accurately calibrate the C peak (284.8 eV) must be performed, and then combine the Gaussian-Lorentzian function to fit data. For the spectrum of C1s in Fig. 6 (a) at 25 °C, it can be divided into two chemical components with binding energies (BE) at 284.8 eV and 286.5 eV, which

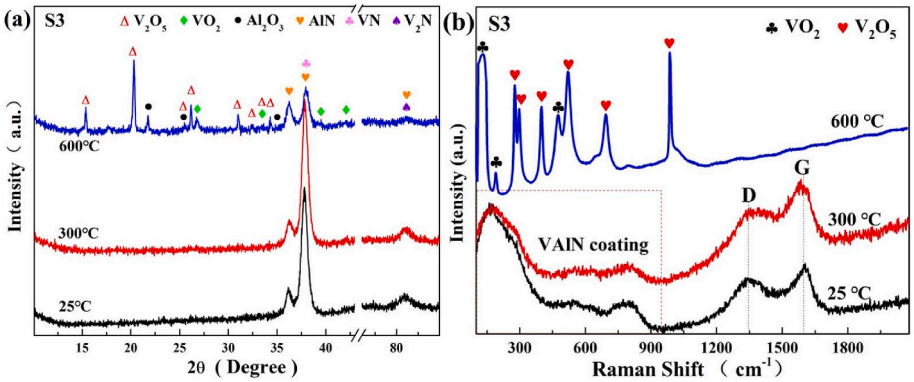

Fig. 5. XRD pattern (a) and Raman pattern (b) of the coating after the tribology test.

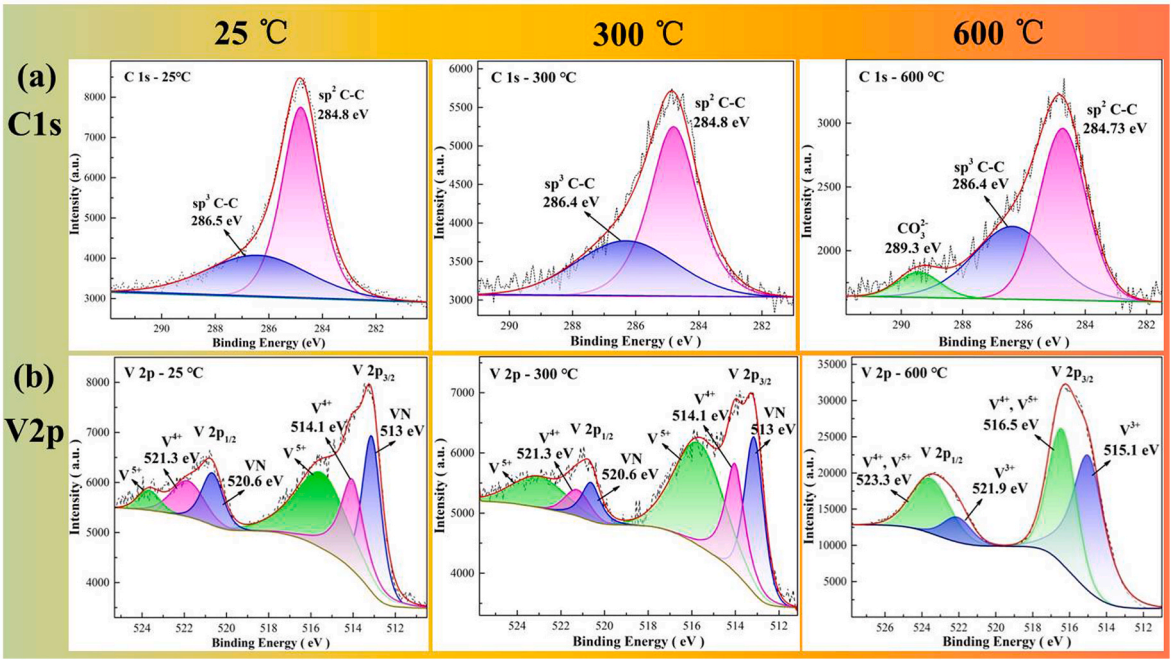

Fig. 6. High resolution XPS spectra of C1s (a) and V2p (b) of coating S3 after friction test at 25 °C, 300 °C and 600 °C respectively.

belong to sp^2 C–C and sp^3 C–C of non-oxygenated carbon [13]. Due to the high thermal stability of graphite, only trace amount of sp^2 C–C bonds are converted to sp^3 C–C after the friction test at 300 °C, which helps to increase the wear resistance and lubricity [24]. In the friction test at 600 °C, C and O are combined to form a carbonyl carbon (C═O) at 289.3 eV due to the influence of the humid and air environment [36]. Throughout the wide temperature range friction process, the content of sp^3 C–C and sp^2 C–C bonds showed an overall downward trend, which means that C is gradually oxidized and disappears on the coating surface and loses its lubricating effect at 600 °C. During the friction process from RT to 300 °C in Fig. 6 (b), the BE at 513 eV and 520.6 eV are belong to VN species, combined with the BE located at 514.1 eV and 521.3 eV, the two main peaks belong to the $V2p_{3/2}$ and $V2p_{1/2}$ orbitals [37], and the only change is the increase of V^{5+} content observed at 515.8 eV and 523.2 eV. After high temperature friction at 600 °C, V^{4+} at 513 eV disappears and turns into a V-based oxide with a valence band higher than V^{3+} [38], which means VN is gradually oxidized and the BE at 515.1 eV and 521.9 eV can be attributed to the V^{3+} species, 516.5 eV and 523.3 eV belong to the V^{5+} oxides [39]. It can be seen from the XPS data that the a-C film and VN phase have great stability from RT to 300 °C. As the friction temperature increases to 600 °C, the VN gradually oxidized to the V_2O_5 and exerts the lubrication effect, and the compound of lubricating phases are responsible for the low friction performance of coatings over a wide temperature range.

3.6. Analysis of the wear track and counterpart ball surface

The surface morphology variation of wear track can reflect the actual friction situation of coatings during the friction process. Fig. 7 (a) is the morphology of the wear track at RT with the width around 83.1 μm, the round protrusions on surface have no significant changes and with 4.9 at.% O (show in Table 1) adsorbed on surface. From the EDS spectrum in Fig. 7 (d), only trace debris of C can be found on the surface of counterpart ball, which was inadequate to form stable lubricating phase to fill the special micro-protrusions, and the relative sliding between hard ceramics resulted in high COF at RT. The wear track becomes wider (124.3 μm) after friction test at 300 °C as shown in Fig. 7 (b), the slight oxidation caused the obviously increase of 14.3 at.% O content shown in Table 1. Due to the positive pressure and horizontal friction force generated by the normal load, the special protrusions were easier ground down to form a dense and smooth wear track, however, the coating remains intact and without peeling off at 300 °C friction process. Simultaneously, the corresponding EDS shows that large agglomeration of a-C film was adhered to the middle and sides of wear track. The surface morphology and EDS spectrum of the counterpart ball in Fig. 7 (e) show that an ideal lamellar a-C transfer film (36.2 at.% C content) was formed during friction process since the rose of W_R [32], which plays a key factor to form the sliding interface and isolate the direct contact between two hard ceramics then tremendously contributes to the low COF. The TEM and mapping of counterpart ball surface after 300 °C friction was shown in Fig. 7(g), in which the uneven thickness of a-C transfer film was rarely identified range from 30 nm to 68 nm. Simultaneously, the layer adhered on the counterpart ball were V/Al-rich elements, which indicate the V/Al materials transferred first at the initial friction.

After friction test at 600 °C, Fig. 7 (c) shows the wear track was extended to 139.4 μm, regularity sheet-like V_2O_5 with a uniform thickness, and partly peeling off can be observed, which infers the increasing contact area, severely oxidation (O content 49.8 at.% show in Table 1) and tribochemical reaction was occurred to form the V_2O_5 liquid lubricating phase full of wear track during friction process of 600 °C, thus the type of friction is adhesive wear and oxidative wear. Meanwhile, the a-C film was oxidized and then disappeared at the high temperature, the V_2O_5 lubricating phase transfers and accumulates on the counterpart ball to form a thick transfer film can be seen from Fig. 7 (f), which was beneficial to reduce and stable the low COF. It is obviously that the a-C transfer film is more effective than the V_2O_5 transfer film in reducing the COF. In addition, AlN is gradually oxidative decomposition (8.2% et al. element and 0.1 at.% N element in Table 1) at 600 °C, which means the nitride coating is prone to tribo-chemical reaction at high temperature to generate oxides. Simultaneously, the V content has increased significantly to 38.4 at.% reveals that the V element is easily diffused to the surface at high temperature. For comparison, the COF of the carbide formed in VAlCN or VCN coating was still reach up to 0.4 at medium temperature [5], but the modified VAlN coating with a-C top-layer will not damage the structure of coating, and can reduce the COF around 0.1 at 300 °C, simultaneously, combined with the V_2O_5 generated at 600 °C to maintain low tribological behavior

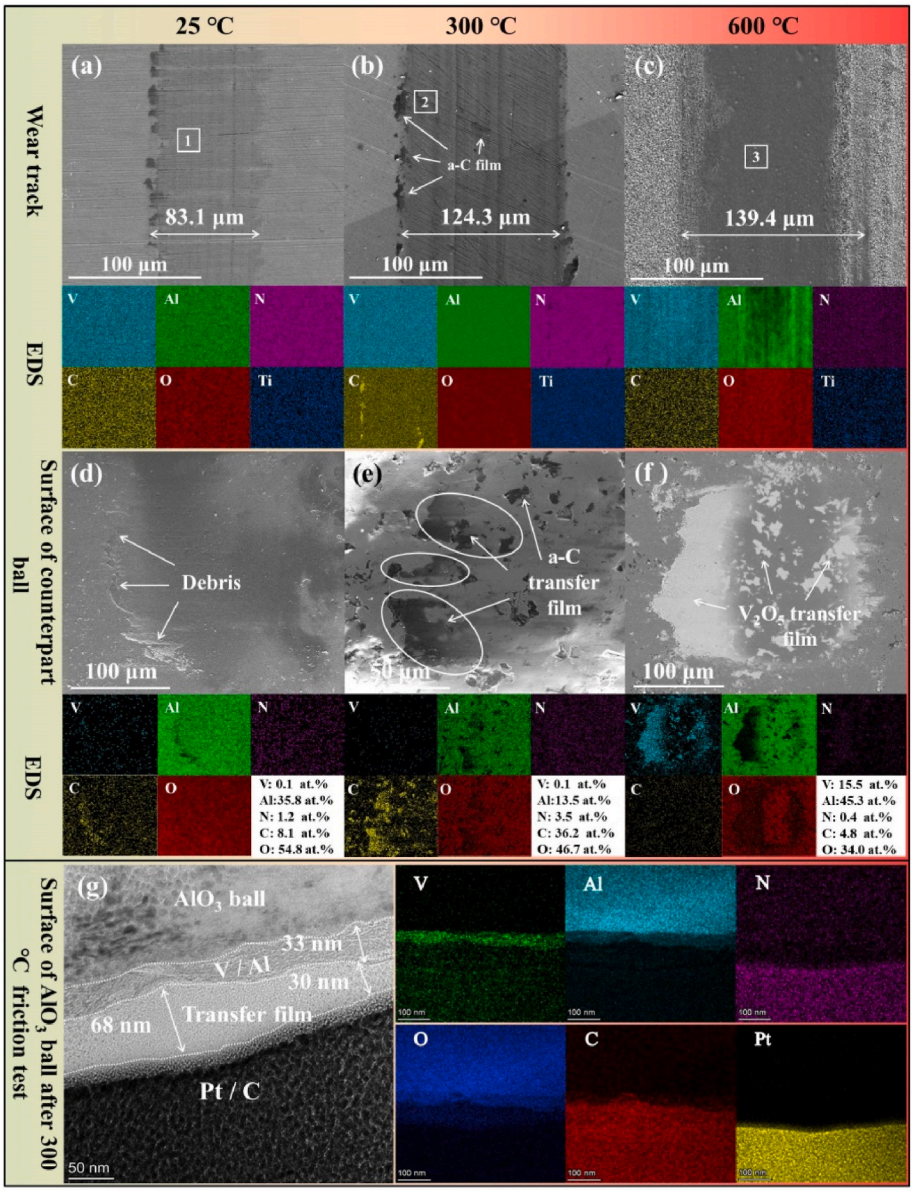

Fig. 7. Morphology (a–c) of wear track and counterpart ball surface (d–f) of S3 coating after friction test at RT, 300 °C and 600 °C; TEM and mapping (g) of the a-C transfer film thickness on counterpart ball.

Table 1
Elements content in the wear track of the S3 coating.

Temperature	Area	Elements (at.%)				
		V	Al	N	C	O
25 °C	1	26.4	26.1	37.9	4.7	4.9
300 °C	2	22.2	21.7	28.6	13.1	14.3
600 °C	3	38.4	8.2	0.1	3.2	49.8

over a wide temperature range.

3.7. The microstructure of coating after friction at 300 °C

The TEM was performed to observe the cross-sectional microstructures of wear track after the friction test at 300 °C. Fig. 8 (a) shows that along the growth direction, there are dense Ti transition layer (0.3 μm), VAlN columnar crystal (1.2 μm) and a-C top-layer (0.09 μm), and a sprayed Pt protective layer. The insert in Fig. 8 (a) shows the SAED of VAlN layer, the polycrystalline diffraction ring belong to AlN phase with lattice indices of (103), (202), (203) and lattice indices of (101), (200) belong to VN phase, which inferred the coating was consisted of polycrystalline structure. The VAlN columnar exhibits high crystallinity observed from the high-resolution TEM (HRTEM) images in Fig. 8 (b) and (c), and the d-spacing of 0.206 nm and 0.237 nm is respectively assign to lattice indices (200) and (111) of VN, and d-spacing of 0.226 nm is assign to lattice indices (002) of V_2N, the d-spacing of 0.14 nm and 0.23 nm are belong to AlN with lattice indices (103) and (101). This result is consistent well with the XRD data in Fig. 3 (a), and shows that the deposited VAlN coating is mainly composed of phases VN and AlN. It is worth noting that the crystal particles wrapped by a-C are observed. From the white line wrapped area and inset SAED in Fig. 8 (d), where the mainly VN (200) and AlN (102) with a lattice spacing of 0.206 nm and 0.18 nm was wrapped in a-C structure. The structure was caused by the oxidized and peeled off protrusions on the top of VAlN coating when the contact surface undergo relative sliding friction. Simultaneously, the counterpart ball gradually aggregates the dispersed a-C film on the coating surface, then forms the lamellar a-C films and wraps the above-

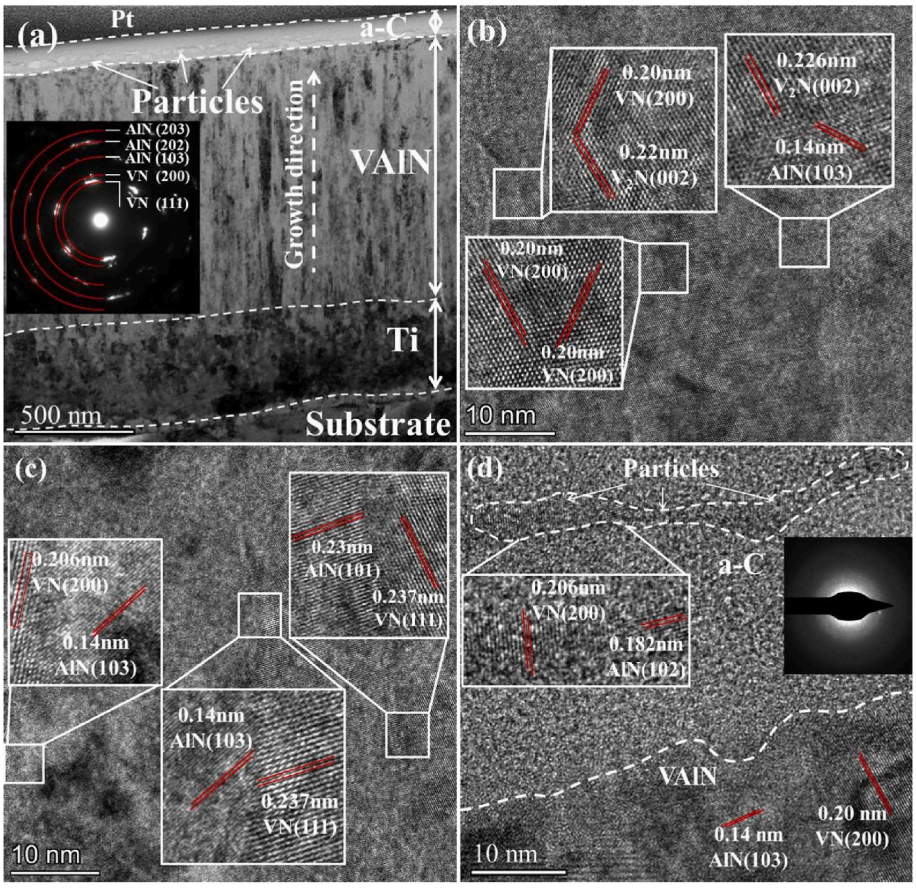

Fig. 8. Cross-sectional TEM (a) and HRTEM images (b), (c) and a-C film (d) of S3 coating.

mentioned granular VN/AlN. This structure plays a role of reducing wear and COF during the friction process over a wide temperature range, especially at a medium temperature of 300 °C.

3.8. Discussion of lubrication mechanism

In order to expound the lubrication mechanism of the VAlN hard ceramic coating modified with intermittent a-C top-layer over a wide temperature range, the friction schematic illustration was drawn in Fig. 9. The low oxidation degree during the friction process at 25 °C fails to soften the protrusions on the coating surface as shown in Fig. 9 (a), so the intermittent a-C film cannot be gathered on the wear track to form the sufficient and large area lubricating film. On the other hand, only trace amount of a-C debris transferred to the contract surface of counterpart ball and the a-C transfer film cannot be formed, thus the relative sliding between hard ceramics results in the high COF. During initial

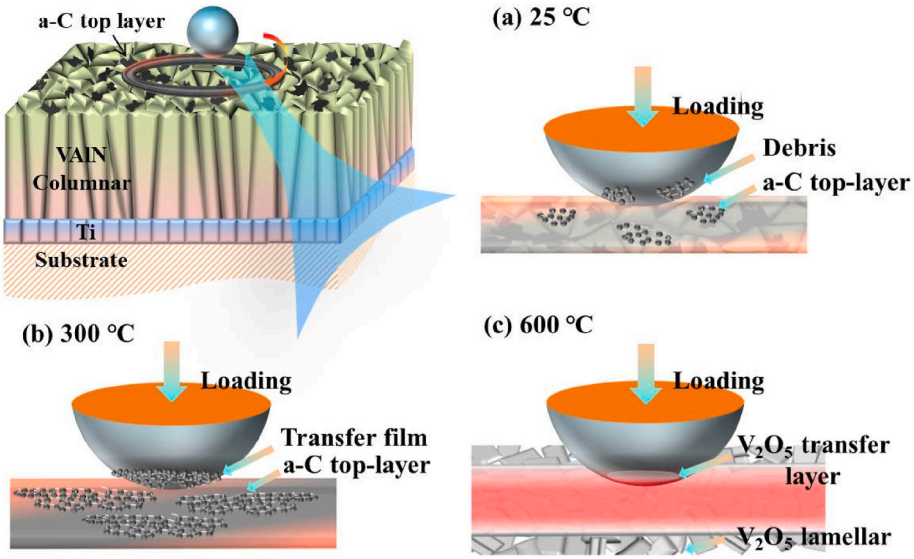

Fig. 9. Schematic of the lubrication mechanism of coating over a wide temperature range.

rotating friction at 300 °C as shown in Fig. 9 (b), due to the positive pressure and horizontal friction generated by the normal load, as well as the oxide effect, the protrusions were peeled off and wrapped in a-C film, afterwards enriched the protrusions gap and formed the smooth wear track. Meanwhile, large agglomeration of intermittent a-C top-layer enable the formation of larger a-C film adhered to the middle and both sides of wear track. Simultaneously, the VAlN layer with high hardness provides a strong supporting effect and not destroyed at 300 °C, also with suitable load was conducive to the formation of a-C transfer film on the contact surface of counterpart ball during the running-in period. The relative sliding occurred between a-C transfer film and residual a-C film on VAlN coating surface, which was conductive to form the ideal lamellar sliding interface at macroscale, thus the lamellar a-C film was obviously the key trigger of the achieved low COF in the friction process at 300 °C. During the friction process at 600 °C as shown in Fig. 9 (c), the regularity sheet-like V_2O_5 with low shear strength formed after the severely oxidation and tribochemical reaction on the wear track. With the occurrence of adhesive wear, a number of V_2O_5 was transferred and formed a thick transfer film on the counterpart ball surface, which was acted as liquid lubricating phase to provide synergistic lubrication and reduce the COF at high temperature environment.

4. Conclusion

In summary, a novel strategy of DCMS technology and post-annealing was proposed to assemble the intermittent a-C top-layer on VAlN coating, which achieved great tribological behavior over a wide temperature range. With decreasing of working pressure, the mechanical properties was significantly enhanced to the highest of H (34.4 GPa) and E (472 GPa). These coatings exhibit excellent self-adaptive tribological behavior from RT to 600 °C. Especially the uneven thickness of a-C transfer film was rarely identified range from 30 nm to 68 nm at 300 °C, then an ideal lamellar sliding interface formed and relative friction occurred between the a-C film on wear track and the transfer film, which tremendously reduced and stabilized the COF at 0.11. It should be noted that a-C top-layer was slightly graphitized and accompanied with the reduced COF, and the formation of a-C transfer film is the main factor of the low COF at 300 °C. The friction type was adhesive wear and oxidative wear during the 600 °C friction process, the formation of V_2O_5 lubricating phase with low shear strength was synergistic with the V_2O_5 transfer film to effectively reduce and stable the COF around 0.36–0.41. In particular, a corresponding lubrication mechanism was proposed to reveal the excellent tribological behavior over a wide temperature range.

Declaration of competing interest

The authors declare that they have no known competing financial interests or personal relationships that could have appeared to influence the work reported in this paper.

Acknowledgement

This research was financial supported by the National Natural Science Foundation of China (51875555,52025014), Hubei Province Technology Innovation Major Project (2020BED007), CAS Interdisciplinary Innovation Team (292020000008), K.C.Wong Education Foundation (GJTD-2019-13).

References

[1] Zhenyu Wang, Guanshui Ma, Linlin Liu, et al., High-performance Cr2AlC MAX phase coatings: oxidation mechanisms in the 900–1100°C temperature range [J], 167, Corrosion Sci. (2020), 108492.
[2] Dominik Ohmer, Qiang Gao, Opahle Ingo, et al., High-throughput design of 211-M2AX compounds [J], Phys. Rev. Mater. 3 (5) (2019), 053803.
[3] Yupeng Zhang, Panpan Li, Ji Li, et al., Tribological properties of MoS2 coating for ultra-long wear-life and low coefficient of friction combined with additive g-C3N4 in air [J], Friction 9 (4) (2020) 789–801.
[4] Yuexiu Qiu, Li bo, Lee Jyh wei, et al., Self lubricating CrVNC coating strengthened via multilayering with VN, J. 21 (5) (2014) 545–550.
[5] Yongtao Mu, Ming Liu, Yongqiang Zhao, Carbon doping to improve the high temperature tribological properties of VN coating [J], Tribol. Int. 97 (2016) 327–336.
[6] M. Aouadi Samir, Jingjing Gu, Berman Diana, Self-healing ceramic coatings that operate in extreme environments: a review [J], J. Vac. Sci. Technol. 38 (5) (2020), 050802.
[7] D. Stone, J. Liu, D.P. Singh, et al., Layered atomic structures of double oxides for low shear strength at high temperatures [J], Scripta Mater. 62 (10) (2010) 735–738.
[8] R. Das, C. Melchior, K.M. Karumbaiah, Self-healing composites for aerospace applications [J], Adv. Compos. Mater. Aerosp. Eng. (2016) 333–364.
[9] Shailesh Kumar, Singh Somnath Chattopadhyaya, A. Pramanik, Sanjeev Kumar, Navendu Gupta, Influence of nano-particle on the wear behaviour of thin film coatings [J], Int. J. Appl. Eng. Res. 13 (6) (2018) 4053–4058.
[10] Yuexiu Qiu, Sam Zhang, Li Bo, et al., Improvement of tribological performance of CrN coating via multilayering with VN [J], Surf. Coating. Technol. 231 (2013) 357–363.
[11] Franz Robert, Mitterer Christian, Vanadium containing self-adaptive low-friction hard coatings for high-temperature applications: a review [J], Surf. Coating. Technol. 228 (2013) 1–13.
[12] Kolozsvári Szilárd, Pesch Peter, Ziebert Carlos, et al., Deposition and characterization of hard coatings in the material system V-Al-N by reactive magnetron sputter deposition [J], Plasma Process. Polym. 6 (S1) (2009) 146–151.
[13] Hao Chen, Xiaohao Xie, Yun Wang, et al., Understanding corrosion and tribology behaviors of VN and VCN coatings in seawater [J], Tungsten 1 (1) (2019) 110–119.
[14] A.V. Bondarev, M. Golizadeh, N.V. Shvyndina, et al., Microstructure, mechanical, and tribological properties of Ag-free and Ag-doped VCN coatings [J], Surf. Coating. Technol. 331 (15) (2017) 77–84.
[15] Nairu He, Hongxuan Li, Ji Li, et al., High temperature tribological properties of TiAlSiN coatings produced by hybrid PVD technology [J], Tribol. Int. 98 (2016) 133–143.
[16] Ping Zhu, Fangfang Ge, Shengzhi Li, et al., Microstructure, chemical states, and mechanical properties of magnetron co-sputtered V1−xAlxN coatings [J], Surf. Coating. Technol. 232 (10) (2013) 311–318.
[17] G. Greczynski, S. Mráz, M. Hans, et al., Unprecedented Al supersaturation in single-phase rock salt structure VAlN films by Al+ subplantation [J], J. Appl. Phys. 121 (17) (2017), 171907.
[18] G. Greczynski, S. Mráz, H. Ruess, et al., Extended metastable Al solubility in cubic VAlN by metal-ion bombardment during pulsed magnetron sputtering: film stress vs subplantation [J], J. Appl. Phys. 122 (2) (2017), 025304.
[19] Xiaowei Li, Aiying Wang, Lee Kwang-Ryeol, Fundamental understanding on low-friction mechanisms at amorphous carbon interface from reactive molecular dynamics simulation, J. Carbon. 170 (2020) 621–629.
[20] Hongxuan Li, Tao Xu, Chengbing Wang, et al., Tribochemical effects on the friction and wear behaviors of a-C:H and a-C films in different environment [J], Tribol. Int. 40 (1) (2007) 132–138.
[21] Young-Jun Jang, Jae-Il Kim, Woo-Young Lee, et al., Friction properties of thick tetrahedral amorphous carbon coating with different surface defects under dry contact conditions [J], 550, Appl. Surf. Sci. (2021), 149332.
[22] Kun Sun, Dongfeng Diao, Current density effect on current-carrying friction of amorphous carbon film, J. Carbon. 157 (2020) 113–119.
[23] Itzel Castillo Müller, Joanne Sharp, Rainforth W. Mark, et al., Tribological response and characterization of Mo–W doped DLC coating, J. Wear 376–377 (2017) 1622–1629.
[24] Zhaobing Cai, Yang Wu, Jibin Pu, High-temperature friction and wear behavior of varying-C VN films [J], J. Mater. Eng. Perform. 30 (3) (2021) 2057–2065.
[25] Zhenyu Wang, Xiaowei Li, Xin Wang, et al., Hard yet tough V-Al-C-N nanocomposite coatings: microstructure, mechanical and tribological properties [J], Surf. Coating. Technol. 304 (8) (2016) 553–559.
[26] Zhenyu Wang, Cuicui Wang, Yupeng Zhang, et al., M-site solid solution of vanadium enables the promising mechanical and high-temperature tribological properties of Cr2AlC coating [J], Mater. Des. (2022) 222.
[27] Xiuqiu Yue, Li Bo, Jyh-wei Lee, et al., Self lubricating CrVNC coating strengthen via multilayering with VN [J], J. Iron. Steel Res. Int. 21 (5) (2014) 545–550.
[28] Xinjie Chen, Du Yao, Chung Yip-Wah, Commentary on using H/E and H/E as proxies for fracture toughness of hard coatings [J], Thin Solid Films 688 (2019), 137265.
[29] Kangsen Li, Gang Xu, Xiaobin Wen, et al., High-temperature friction behavior of amorphous carbon coating in glass molding process [J], Friction 9 (6) (2020) 1648–1659.
[30] Moolsradoo Nutthanun, Shinya Abe, Shuichi Watanabe, Thermal stability and tribological performance of DLC-Si–O films [J], 2011, Adv. Mater. Sci. Eng. (2011) 1–7.
[31] F.L. Freire Jr., G. Mariotto, R.S. Brusa, et al., Structural characterization of amorphous hydrogenated carbon and carbon nitride films deposited by plasma-enhanced CVD [J], Diam. Relat. Mater. 4 (1995) 499–502.
[32] Xingrui Deng, Kousaka Hiroyuki, Takayuki Tokoroyama, et al., Tribological behavior of tetrahedral amorphous carbon (ta-C) coatings at elevated temperatures [J], Tribol. Int. 75 (2014) 98–103.

[33] S. Bhowmick, M.Z.U. Khan, A. Banerji, et al., Low friction and wear behaviour of non-hydrogenated DLC (a-C) sliding against fluorinated tetrahedral amorphous carbon (ta-C-F) at elevated temperatures [J], Appl. Surf. Sci. 450 (2018) 274–283.
[34] Wenzhe Wang, Jibin Pu, Zhaobing Cai, et al., Insights into friction properties and mechanism of self-lubricating MoVN–Ag films at high temperature [J], 176, Vacuum (2020), 109332.
[35] Chunzi Zhang, Qiaoqin Yang, Koughia Cyril, et al., Characterization of vanadium oxide thin films with different stoichiometry using Raman spectroscopy [J], Thin Solid Films 620 (2016) 64–69.
[36] Bhavana Gupta, Niranjan Kumar, Alexey Titovich Kozakov, et al., Lubrication properties of chemically aged reduced graphene-oxide additives [J], Surface. Interfac. 7 (2017) 6–13.
[37] Hongjian Zhao, Zenglei Ni, Mi Pengbo, et al., The microstructure and phase evolution of cone-like VN coating in a wide temperature range [J], Surf. Coating. Technol. 307 (A) (2016) 151–156.
[38] Ureña-Begara Ferran, Crunteanu Aurelian, Raskin Jean-Pierre, Raman and XPS characterization of vanadium oxide thin films with temperature [J], Appl. Surf. Sci. 403 (2017) 717–727.
[39] A. Glaser, S. Surnev, F.P. Netzer, et al., Oxidation of vanadium nitride and titanium nitride coatings [J], Surf. Sci. 601 (4) (2007) 1153–1159.